J Mater Sci (2020) 55:13457–13471

Polymers & biopolymers

Experimental characterisation and modelling of mechanical behaviour of microcapsules

A. Aniskevich[1,*], V. Kulakov[1], O. Bulderberga[1], P. Knotek[2], J. Tedim[3], F. Maia[4], V. Leisis[5], and D. Zeleniakiene[5]

[1] *Institute for Mechanics of Materials, University of Latvia, Riga, Latvia*
[2] *Faculty Chemical Technology, Department of General and Inorganic Chemistry, University of Pardubice, Pardubice, Czech Republic*
[3] *CICECO/DEMaC, Universidade de Aveiro, Campus Universitário de Santiago, 3810-193 Aveiro, Portugal*
[4] *Smallmatek-Small Materials and Technologies Lda, Aveiro, Portugal*
[5] *Department of Mechanical Engineering, Kaunas University of Technology, Kaunas, Lithuania*

Received: 3 February 2020
Accepted: 7 June 2020
Published online: 19 June 2020

© Springer Science+Business Media, LLC, part of Springer Nature 2020

ABSTRACT

Results of experimental characterisation and modelling of mechanical behaviour of microcapsules for self-sensing polymer composites are presented. Melamine–formaldehyde microcapsules were selected for this purpose. The average diameter, size distribution, and shell thickness of microcapsules were evaluated from scanning electron microscopy images. Compressive properties of the shell material were evaluated in several ways. AFM measurements allowed estimating stiffness and strength of a single microcapsule. In parallel, modelling of the mechanical behaviour of a single microcapsule was performed. Buckling of a thin-walled spherical shell under external pressure was considered and closed-form solution in a linear statement was obtained. The results of analytical calculations were compared with FEM modelling. Two demonstrator thin-shells with the radius of centimetre scale, hollow and filled with water, were tested in compression between two rigid plates. The results of their numerical analysis obtained by FEM models developed are in good agreement with experimental results.

Introduction

Polymer composites are widely used in aviation, automotive, wind power industries where structural members are subjected to high loads. Structural health monitoring is a topical issue for such constructions [1]. The non-destructive testing methods such as sensors embedded into structural members during their manufacture allow one to assess a state of the structure during its operation through continuous monitoring [2, 3]. However, these sensors embedded into the material lead to the drastic decrease of its mechanical properties [4].

Address correspondence to E-mail: andrey.aniskevich@pmi.lu.lv

https://doi.org/10.1007/s10853-020-04925-8

Recently, the concept of using the microcapsules as sensors for the controlled release of high-performance polymeric coatings is one of the most relevant [5]. This concept is based on the combination of the active protection with sensing functionalities that indicate when the protective coating is damaged, and the substrate is already under the risk. Such smart self-sensing composite structures are capable to provide the information about structural integrity.

The design of smart structural composites with microcapsules (MCs) embedded in various layers, which provide the extra functions of self-healing [6–15] or detection of damages arising under an influence of external forces [1, 5, 16–21], is a promising direction in the mechanics and technology of composites that has been actively developed in recent decades. This concept is based on the destruction of microcapsules embedded in the smart composite at a certain level of the applied external load and a release of healing or colouring agents from them. Self-healing technology is used not only to recovering the mechanical characteristics of damaged composites but also their electrical conductivity [22]. The design of such smart composites is a complex scientific and technological problem, including the development of the microcapsules themselves, their effective embedding into the smart composites, and characterisation of the mechanical properties of microcapsules and the smart composites themselves.

The generation of effective smart composites requires the investigation of a large number of factors affecting their physical and mechanical properties. These are primarily the geometric and mechanical characteristics of the microcapsules themselves. Microcapsules commercially manufactured by various methods are often polydisperse with respect to the diameter and thickness of the shell, but the possibility to control these parameters in the existing processes is limited [23]. Therefore, a gravimetric analysis of the microcapsules used is required. The generation of effective smart composites requires also an understanding of the mechanical behaviour of microcapsules, especially their failure behaviour and the magnitudes of ultimate loads [23–31].

The mechanical properties of microcapsules can be determined by various experimental methods, studying both an ensemble of microcapsules and a single one. In the first case, some averaged value of the characteristic is measured. In latter, the mechanical tests carried out with a single microcapsule provide more detailed information about its deformation and strength properties. For this purpose, the most commonly used test is the compression of a microcapsule between two parallel plates (see e.g. [23–25].) and experiment on microcapsule nanoindentation by using an atomic force microscope (AFM) [23, 24, 26]. The advantage of the latter method is the ability to carry out the high-resolution mechanical tests in the range of small forces of nanoindentation and strains comparable with the thickness of microcapsules. Mechanical forces easily deform the thin-walled capsules and variation of an interior or external pressure can lead to their buckling. Some researchers use this mechanical behaviour of microcapsules for experimental evaluation the elastic modulus of their shell material [24, 29, 32].

From the viewpoint of structural mechanics based on continuum theory, the microcapsules are considered as thin-walled shells, the mechanical loading of which, as a rule, is accompanied by the development of large displacements, strains, and nonlinear character of deformation [27]. Besides, they, like thin-walled shells, are extremely sensitive to an initial imperfection of shape and failure due to loss of stability [23]. Therefore, analytical solutions of the problems concerned with the determination of their stress–strain state are possible in rare cases or with significant simplifying hypotheses. As follows from the studies published [23, 24, 26], a good agreement between the experimental results and numerical calculations provides finite element modelling (FEM) of the process of deformation of microcapsules.

Making predictions of the mechanical behaviour and response of these self-sensing structures with microencapsulated active materials embedded into polymer matrices by numerical simulations is a good possibility to understand a real phenomenon at the micro-level of the composites and cannot be implemented in the existing analytical models. Numerical finite element studies were successful for similar problems such as control of stress concentration near-spherical capsule with internal pressure embedded into polymeric material [33] or insights of stress distribution in heterogeneous microstructure of polymer blends with spherical inclusions [34].

In view of the foregoing, the objective of the present investigation was to predict the mechanical properties of microcapsules for self-sensitive polymer composites independently of their chemical nature, giving focus on the microcapsules geometry. The first

stage of the investigation involved the experimental characterisation of the geometrical and mechanical properties of a single microcapsule. An important aspect of our investigation is an understanding of the features of mechanical behaviour of the hollow and liquid-filled microcapsules in compression. The implementation of such experiments directly on microcapsules is very laborious and requires expensive special equipment [35]. However, no absolute length scale enters the theoretical description of shell deformation and the experiments on the macroscopic objects (for example, a ping-pong ball) are well-suited for testing mechanical models [24]. Therefore, at the first stage, we carried out an experimental assessment of the features of deformation in compression between two steel plates on the demonstration models of thin-walled hollow and filled shells having a centimetre scale dimension. Comparison of the experimental results obtained for the demonstration models with the numerical calculations of their stress–strain state performed by FEM allowed us to estimate effectiveness of this numerical method and use it in a subsequent study directly to the calculation of microcapsules.

Materials and methods

Melamine–formaldehyde (MF) microcapsules with leuco dye (MCD) and with dye activator (MCA), as water-based dispersions were supplied by Papierfabrik August Koehler Ag., Germany. The nominal concentration of the microcapsules in the dispersion is approximately 40 mass % (data from the manufacturer).

Samples of shell materials (nitrocellulose, polyethylene terephthalate PET, and gelatine) were cut from the commercial products (like a table tennis ball, thin-walled closed cylindrical PET shell, and gelatine capsule) that were considered as the model shells. Along with some polymer matrices (polyvinyl acetate, epoxy), the shell materials were tested and are described in other Sections of the paper.

Mechanical tests in tension and compression were performed on universal testing machine Zwick Roell 2.5 kN at loading rate from 0.5 to 10 mm/min depending on kind of test and sample size (specified in appropriate Sections).

Scanning electron microscope (SEM) Hitachi S-4100, particle size analyser Coulter LS-230, AFM ICON (Bruker), and NEXT AFM (NT-MDT) were used in the research and mentioned in different Sections.

Experimental characterisation of a single microcapsule

Microscopy of microcapsules

The geometrical characterisation of microcapsules is quite necessary for understanding and successful modelling of their mechanical behaviour. Agglomerated capsules in water-based dispersions were separated by ultrasonic method. Images of single and agglomerated capsules were obtained by a scanning electron microscope (SEM) Hitachi S-4100. The size distribution of microcapsules as calculated by the images processing in automatic and manual modes using ImageJ software (NIH Image) [36]. The program in the automatic mode could not always exactly distinguish a single capsule and capsules agglomerate. Therefore, the results were rechecked in the manual mode (see Fig. 1). Microcapsule size distribution obtained from Fig. 1 treatment is presented in Fig. 2.

Summarizing, it could be concluded that capsules have some distribution by size with an average diameter of MCD equalled to $D = 7 \pm 0.5$ μm and MCA equalled to $D = 2 \pm 0.2$ μm (both results of SEM photo developed manually at least 50 different particles). The size distribution of MCD and MCA was measured by the particle size analyser Coulter LS-230. Automatic counting by ImageJ and results of light scattering measurements give essential errors because of incorrect treatment of microcapsule agglomerates.

For the evaluation of the microcapsules' shell thickness, SEM images of capsules preliminary broken with a scalpel were analysed (see Fig. 3). The average shell thickness determined from six measurements of broken microcapsules was $h = 0.10 \pm 0.01$ μm.

Mechanical properties of microcapsules

AFM and nanoindentation of a single microcapsule

The topography of the dried microcapsules was monitored by atomic force microscopy (AFM) ICON,

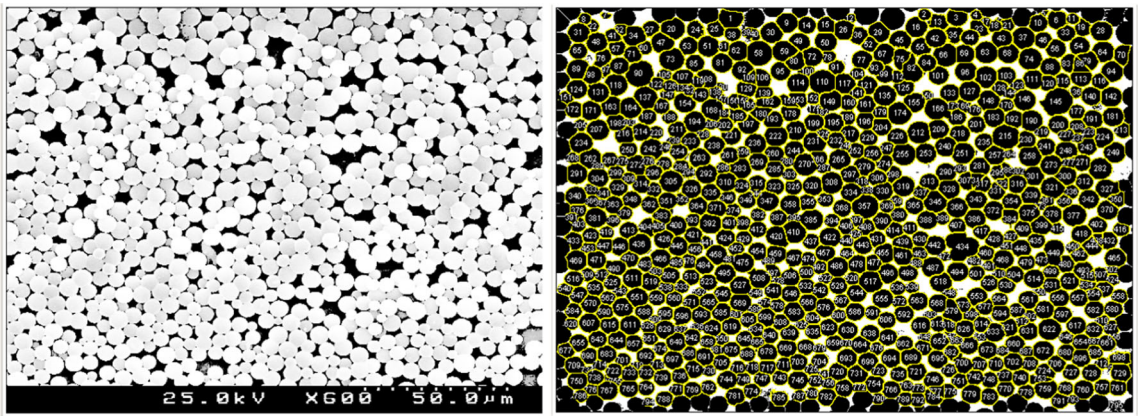

Figure 1 SEM image of MCD (left) and ImageJ processed (right).

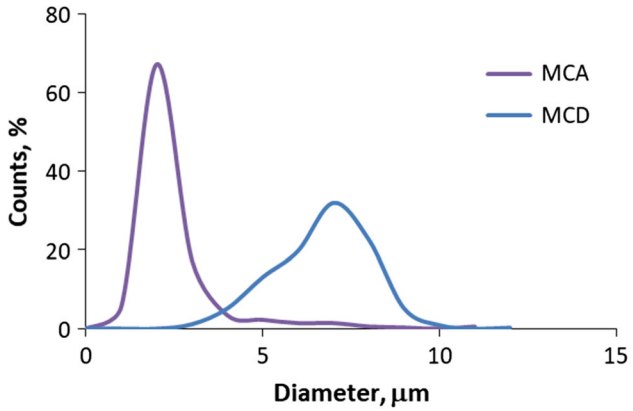

Figure 2 The size distribution of MCA and MCD obtained by photos treatment in ImageJ.

Bruker using mica as a substrate. The separated microcapsules of MCA kept their original almost spherical shape after drying with 1.6 µm height and 1.8 µm width (see Fig. 4).

Nanoindentation measurement was carried out at room temperature with an NEXT AFM (NT-MDT, Russia) equipped with nanoindentation set-up and acoustic shelter. The indenter was a diamond Berkovich tip having three-sided pyramid with a half angle of 30° with a nominal tip apex radius of curvature less than 30 nm and spring constant 10.2 ± 0.3 $kN \cdot m^{-1}$.

The nanoindentation measurement was used for determining the maximal force of loading required for microcapsule rupture and the real quantification of elastic modulus. Typical nanoindentation force-strain diagram of loading up to rupture of the microcapsule is shown in Fig. 5. The force quickly decreased at the microcapsule rupture which was observed on the microscope. The mean load required for rupture was determined as $F^* = 107 \pm 10$ µN.

The value of the elastic modulus was calculated by applying the equation for shallow spheres found by Reissner [24]. The force F required for normal displacement d of the pole under point loading is equal to:

$$F = \frac{h^2}{R} \cdot \frac{4E}{\sqrt{3(1-\nu^2)}} \cdot d \qquad (1)$$

where E is the elastic modulus of microcapsules' shell material, ν is the Poisson's ratio, h is the shell thickness, R is the radius of the capsule. For use of thin-walled shell theory, the shell thickness has to be

Figure 3 Images of damaged microcapsules.

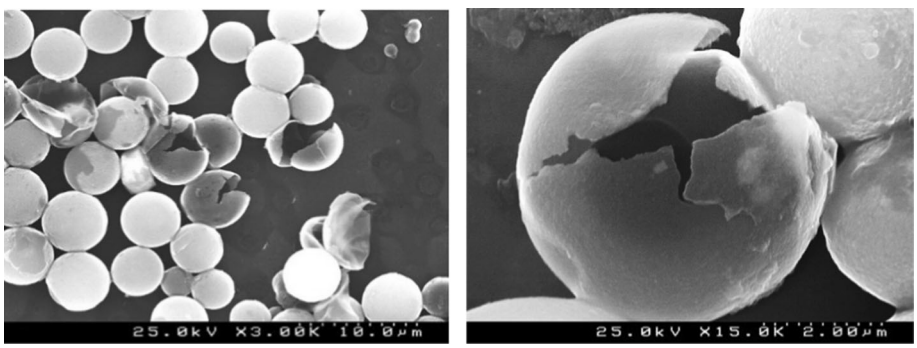

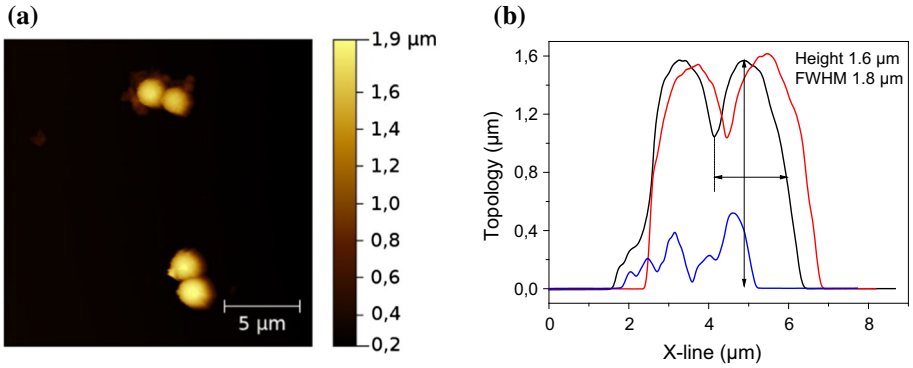

Figure 4 Topological image **a** and corresponding topological profile **b** of microcapsules.

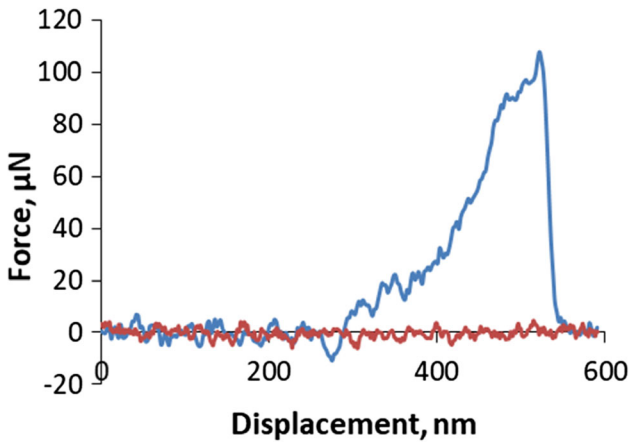

Figure 5 Displacement vs. applied force up to the rupture of the microcapsule on AFM. Loading (blue line) and unloading (orange line).

thin and satisfy the inequality $h/R < 0.1$; the ratio of the radius of loading area r to the outer radius is quite small $r/R << 1$; strains are small compared with the outer radius of the spherical shell.

The calculation was done from the linear part of the nanoindentation curve (small displacement regime). The values of the force of 2.1 µN and displacement of 40 nm (see Fig. 6) and h = 0.1 µm were used. The Poisson's ratio ν = 0.3 was used [6]. Elastic modulus of shell material for the individual microcapsule with the diameter of D = 1.5 µm was estimated using Eq. (1) as E = 1.6 GPa. The same procedure was carried out on the ten individual microcapsules and the mean elastic modulus was determined $E = 1.7 \pm 0.2$ GPa.

Compression testing of microcapsules' shell material

Two series of samples of shell materials have been manufactured and tested to determine the macroscopic mechanical properties in a direct way. The first series of bulk samples of polymer resin based on MF resin was made in the laboratory using an adapted protocol from the literature [37], and the resulting materials present the expected chemical properties [37]. Briefly, microcapsules polymerisation was performed by interfacial polycondensation of MF resin and crosslinking agent (Saduren® 163, gently provided by BASF SE, Germany) in acidic conditions with pH ≈ 4 and temperature from 85–90 °C, during 2 h. During the heating process, acetic acid and the catalyst $MgCl_2$ were added to favour the polymerisation. The mixture was mixed for 40 min before polymerisation occurred and in 10 min almost all pre-polymer got very viscous. Viscous material was removed from the reaction media and placed to rest in a dry room for 15 h. Slabs of 4 × 4 × 3 mm were cut from the resin. Quasi-static compression tests of the samples were performed under the test speed of 0.5 mm/min. Tests were carried out for two groups of 3–4 replicate samples with compression force applied in the manufacturing direction for one group of samples and in the transversal direction for another one. The quasi-static compression test

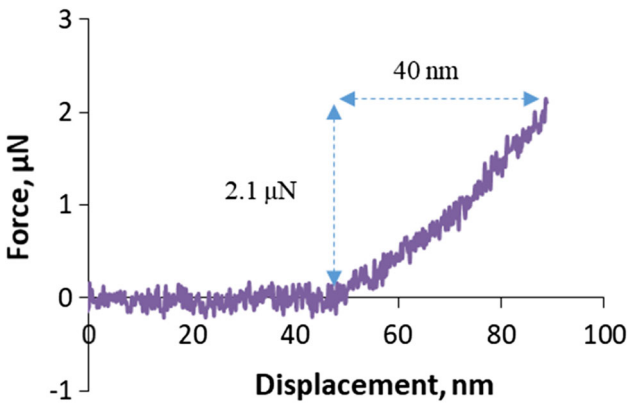

Figure 6 Nanoindentation curve in the small displacement regime.

diagrams are presented in Fig. 7. Average values of the elastic modulus were estimated as $E = 640 \pm 50$ MPa and compressive strength $\sigma^* = 40 \pm 8$ MPa for sample along manufacturing direction, and $E = 490 \pm 70$ MPa and $\sigma^* = 40 \pm 3$ MPa for transversal one.

The second series of shell material was supplied from the microcapsules manufacturer (Koehler Ag.). Microcapsule shell material was also made from melamine–formaldehyde resin. Two types of the shell material were supplied: (*A*) Pure shell material resin (cross-linked), (*B*) Shell material and additives used for microencapsulation (cross-linked). The properties of real shell material of microcapsules have to be intermediate between the properties of *A* and *B* due to the specific industrial technological processes. Samples of the material were supplied in jelly-like form and they become brittle after the complete drying and had an irregular form. The cross section area of the samples was calculated optically by treating the photos in Adobe Photoshop® software. Samples of both types were tested in compression at a cross-head test rate of 0.5 mm/min with a cylindrical indenter of 6.10 ± 0.15 mm diameter and between two plates.

Totally, 34 samples were tested: with indenter—shell material *A* (5 samples), shell material *B* (9 samples); without indenter—shell material *A* (10 samples) and shell material *B* (10 samples). Typical stress–strain diagrams for the shell material *A* and shell material *B* with and without indenter are presented in Fig. 8. The values of Young's modulus *E*, strength σ*, and ultimate strain ε* for shell material *A* and *B* averaged over the series of the compression tests are presented in Table 1.

Comparison of the results of compression tests with indenter and between two plates (see Table 1) shows that both methods give similar results within the standard deviation. Thus, Young's modulus for the real shell material of microcapsule is expected in the range approx. between 20 and 60 MPa.

Besides, the elastic properties of microcapsules obtained experimentally from nanoindentation and macroscopic compression tests are essentially different. Microcapsules filled with liquid behave a complex mechanical structure. Their compressive properties strongly depend on the properties of the shell material that on the other hand also depend on the technology of manufacturing and testing environment.

Modelling of mechanical behaviour of a single microcapsule

Modelling of mechanical behaviour of a single microcapsule was motivated by two reasons. Firstly, elastic properties and strength of MC have to be controlled by the manufacturer to provide the necessary functionality of MC. In a case of damage indication, MC has to be broken at a given mechanical load level which has to be predicted in advance during the design stage using mechanical models. Secondly, MC placed in a polymer matrix could be considered as a specific filler of a composite material changing its mechanical properties. These changes

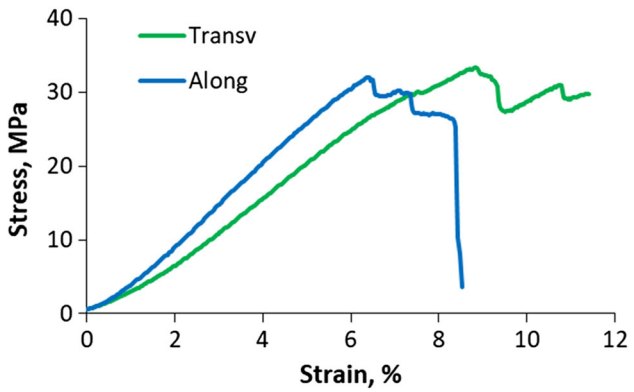

Figure 7 Typical diagrams of quasi-static compression tests for along manufacturing (blue) and transversal (green) directions of MF samples.

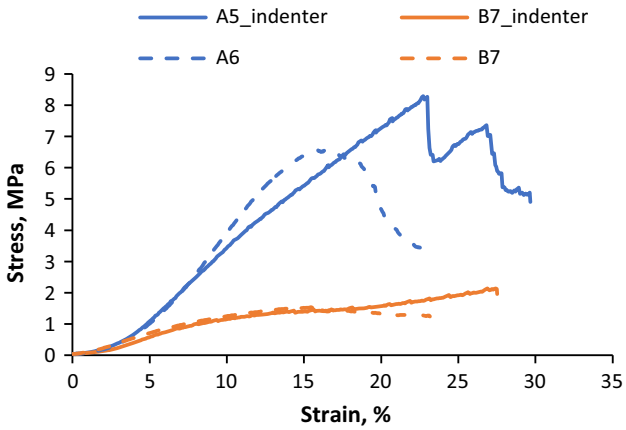

Figure 8 Typical stress–strain diagrams for the shell materials A (blue lines) and B (orange lines) in compression with indenter (solid lines) and two plate's compression (dashed lines).

Table 1 Averaged values of mechanical properties of shell materials *A* and *B* in the compression tests

Material	Test method	*E*, MPa	σ*, MPa	ε*, %
A	Indenter	53 ± 8	8.1 ± 0.7	20 ± 2
	Two plates	61 ± 16	6.2 ± 1.4	13 ± 2
B	Indenter	19 ± 3	2.6 ± 0.2	12 ± 4
	Two plates	17 ± 1	1.5 ± 0.1	15 ± 1

strongly depend on the properties of the material of MC if all other parameters are the same. To predict the properties of the polymer matrix filled with MC, the properties of the latter have to be known.

Buckling of a thin-walled spherical shell under external pressure

The mechanical behaviour of microcapsules could be modelled as the behaviour of thin-walled shells. During the exploitation of MC in a polymer matrix, one of the most possible kinds of mechanical loads is external pressure and MC buckling is a critical point that restricts these loads. This is why buckling of a thin-walled spherical shell under external pressure has to be considered.

Closed-form solution in linear statement

Let us consider a problem of stability of a hollow spherical shell with a radius of curvature of the middle surface R and wall thickness h loaded by uniformly distributed external pressure q (see Fig. 9) in the linear statement neglecting the quadratic terms of the displacements of the shell in the governing equation of its bending.

The sub-critical steady state of the shell considered is described by the following forces and stress:

$$N_\alpha^0 = N_\beta^0 = N^0 = \frac{qR}{2},\ N_{\alpha\beta}^0 = 0; \sigma = \frac{qR}{2h} \tag{2}$$

Radial displacement w_0 of all points of the middle surface of the shell, which corresponds to the initial stress σ, is calculated as

$$w_0 = \varepsilon R = \sigma R \frac{(1-\nu)}{E} = \frac{qR^2(1-\nu)}{2Eh}. \tag{3}$$

With increasing of the external pressure q, a local dent is originated on the surface of the sphere at some instant of time. Further, the additional deflection associated with local buckling will be denoted as w.

We assume that the spherical shell within the region of this initial dent can be considered as a swallow one and its bending behaviour can be described by the following linearised governing equation [38]:

$$D\nabla^2\nabla^2\nabla^2 w + \sigma h \nabla^2\nabla^2 w + \frac{Eh}{R^2}\nabla^2 w = 0, \tag{4}$$

where $\nabla^2 = \frac{\partial^2}{\partial x^2} + \frac{\partial^2}{\partial y^2}$, $D = \frac{Eh^3}{12(1-\nu^2)}$ is the bending stiffness of the shell, E and ν are the modulus of elasticity and Poisson's ratio of the shell material, respectively.

Following Vlasov's assumption [39], we accept that a buckling mode of a thin-walled spherical shell is described by the equation for Bessel function of the first kind

$$\nabla^2 w = -\lambda^2 w, \tag{5}$$

where λ is an undetermined parameter.

By virtue of the assumption (5), we reduce Eq. (4) at $\lambda \neq 0$ to the following simplified form:

$$\sigma = \frac{D}{h}\lambda^2 + \frac{E}{R^2\lambda^2}. \tag{6}$$

Minimum of the function $\sigma = \sigma(\lambda^2)$ is attained when

$$\lambda^2 = \sqrt{\frac{Eh}{DR^2}} = \frac{\sqrt{12(1-\nu^2)}}{Rh}. \tag{7}$$

The substitution of the relation (7) into (6) allows us to obtain the following formulas for the critical buckling stress σ_{cr}, critical pressure q_{cr}, half-wavelength of buckling L_w, and the number of buckling waves N_w:

$$\sigma_{cr} = \frac{E}{\sqrt{3(1-\nu^2)}}\frac{h}{R},\ q_{cr} = \sigma_{cr}\frac{2h}{R} = \frac{2E}{\sqrt{3(1-\nu^2)}}\frac{h^2}{R^2},$$
$$L_w = \frac{\pi}{\lambda} = \pi\sqrt[4]{\frac{R^2h^2}{12(1-\nu^2)}},\ N_w = \frac{\pi R}{L_w}. \tag{8}$$

Numerical example. Let us specify that R = 2 μm, h = 0.1 μm, E = 5 GPa, and ν = 0.3. In this case, the closed-form solution derived (7) gives us the following values of the critical magnitudes: q_{cr} = 9.68 MPa, σ_{cr} = 121.05 MPa, L_w = 0.864 μm, and $N_w \approx 9$.

It has to be noted that the real thin-walled hollow shells are very sensitive to a slight imperfection of their geometry and non-axial symmetry of external load application. Due to a presence of any geometric

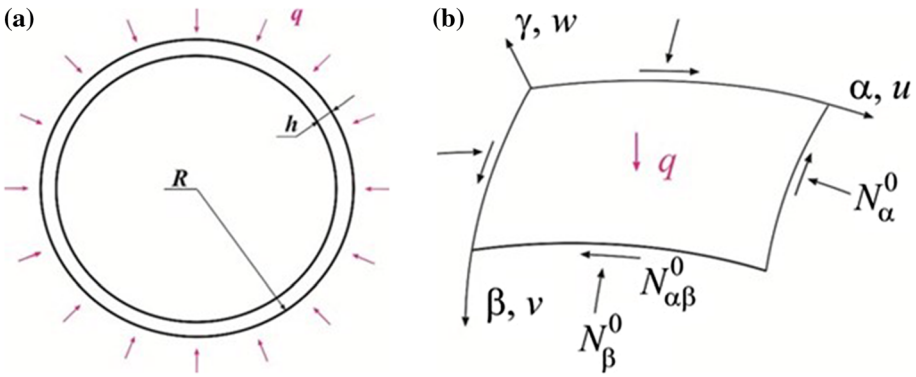

Figure 9 The geometry of a spherical shell **a**, the displacements u, v, w, and internal forces N^0_α, N^0_β, and $N^0_{\alpha\beta}$ operating in the directions of curvilinear axes α, β, and γ **b**.

imperfection of the shape and not strictly axisymmetric loading, the real thin-walled elastic shell changes its initial shape with increasing the external load. Their loss of stability, as a rule, occurs in a snap-through mode and the true value of the critical force is usually much lower than calculated with help of the linear theory of buckling considered.

For this reason, three characteristic values of critical load can be distinguished for the thin-walled elastic shells, namely, upper, lower, and true ones [40]. In the case considered, they are upper q_{1cr}, lower q_{2cr}, and true q_{snap} values of external pressure q.

- The upper value q_{1cr} corresponds to a shell of an ideal shape (without any imperfection) and is determined by solving the linearised governing equation of shell bending (3).
- The lower value q_{2cr} corresponds also to a shell of an ideal shape (without any imperfection) but is determined by solving numerically the nonlinear buckling problem.
- The true value q_{snap} corresponds to a real shell with any geometrical imperfection and is determined experimentally at an instant of the shell buckling in a snap-through mode.

These three characteristic values of critical loads satisfy the following inequality:

$$q_{2cr} < q_{snap} < q_{1cr}. \tag{9}$$

As a rule, upper critical pressure q_{1cr} is three or four times greater than the lower one q_{2cr}. The true value of the critical load q_{snap} depends on a degree of imperfection of the geometric shape of the shell and non-axial symmetry of its loading.

Finite element solution

Only a few problems concerned with deformation of the thin-walled elastic spherical and cylindrical shells can be solved analytically with deriving the closed-form solutions, especially with accounting for nonlinear effects of their deformation. The buckling problem of a thin-walled hollow spherical shell under external pressure has the closed-form solution and this gives us a possibility to compare the results obtained by this solution and numerically calculated by using the finite element method (FEM). This comparison enables us to estimate the effectiveness of FEM application for modelling the deformation of a thin-walled hollow spherical shell.

Finite element (FE) model for the thin-walled hollow spherical shell with the geometrical and elastic characteristics specified in the *numerical example* was constructed by using software ANSYS Mechanical 12.1. Due to symmetry of the shell geometry and its loading condition, we can consider only a hemisphere of the shell and create FE model by using 2D finite elements PLANE 183. The buckling problem is solved in two successive steps of loading.

- The first step is concerned with preloading by unit force F, which generates a local dent on the shell surface (Fig. 10a).
- The second step is concerned with the application of external pressure q, which buckles the shell reaching the critical value q_{cr} (Fig. 10b).

The critical value q_{cr}^{FEM} calculated by FEM for the shell with the geometry and elastic characteristics considered is equalled to 9.79 MPa. Thus, the difference of 1.12% between the critical values calculated by FEM and closed-form solution proves the effectiveness of FEM application for describing the

mechanical behaviour of the thin-walled hollow spherical shells under external pressure.

Compression of a thin-walled spherical shell between two rigid plates

The analytical and/or FE models describe a deformation of thin-wall shells independently of their absolute length scale, therefore the experiments made on their macroscopic models are well-suited for testing mechanical models [24].

The difference in the behaviour of the hollow system (empty capsule shell) and the system filled with liquid (a filled MC) under the compression load should be also checked for a model system. Let us consider the deformation behaviour of several model shells partially compliant with the requirements formulated.

The first model was *table tennis ball* (TTB) in compression between two steel plates (Fig. 11a). The hollow thin-walled shell and the shell filled with a practically incompressible medium were considered. For half model of the ball, the symmetry boundary conditions were used and FE mesh was generated (Fig. 11b). Shell middle radius was R = 20 mm, shell thickness h = 0.4 mm, h/R = 0.02.

Tensile tests of nitrocellulose samples were performed to determine the elastic modulus of the shell material. Five samples of the strip and dog bone shape samples were cut from TTB shell and tested with crosshead displacement rate 2 mm/min (see diagrams in Fig. 12). The average value of elastic modulus was evaluated as $E = 1.80 \pm 0.15$ GPa. Poisson's ratio was assumed $\nu = 0.3$ from [41].

The nonlinear contact problems of compression of the hollow and filled TTB between two rigid plates were solved numerically by using FEM modelling with the help of finite element software ANSYS Mechanical 12.1.

Due to the axial symmetry of the shell geometry and loading condition, only a hemisphere of TTB was considered. The TTB was meshed by 2D finite elements PLANE 183. To model contact between the outer surface of TTB and the top surface of the bottom steel plate, these contact surfaces were meshed by contact elements CONTA 171 and TARGE 169, respectively. Compressive action of the top steel plate was modelled as the application of the pressure on the cross sections of the hemisphere whose value was corresponded to the maximum displacement of the top plate equalled to 10 mm. The initial configuration and the deformed one, corresponding to the

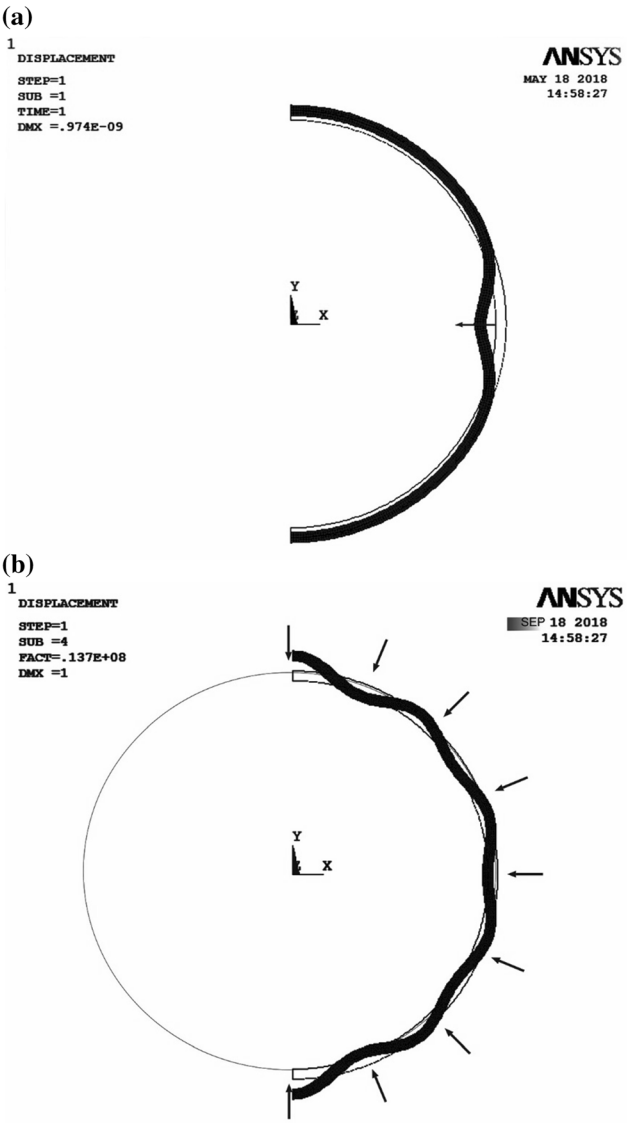

Figure 10 Deformed configurations of the shell after preloading **a** and buckling under external pressure **b**.

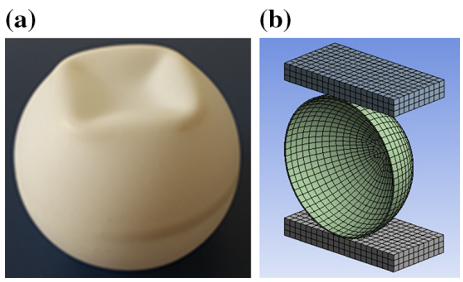

Figure 11 Verification of models: the deformed shape of a table tennis ball **a,** FE model **b**.

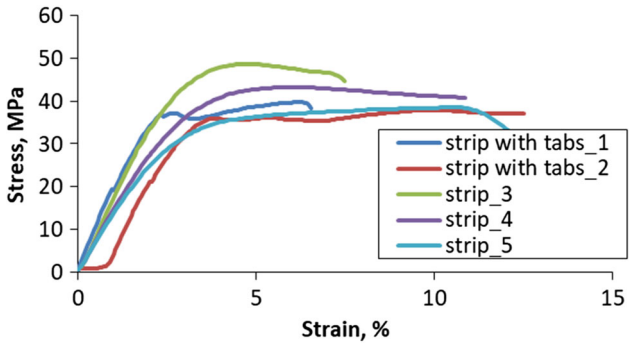

Figure 12 Tensile diagrams of TTB shell material (nitrocellulose) samples.

maximum displacement of 10 mm of the top steel plate, are shown in Fig. 13.

The results of the simulation of the compression behaviour of hollow TTB shell are discussed below. FE modelling of the TTB filled with a practically incompressible medium is illustrated by the data of Fig. 14. Filler of the shell was considered as a medium with the following elastic properties: E_f = 20.0 MPa, ν_f = 0.49967. Creating the FEM models for the filled TTB, we consider only a quarter of their cross sections owing to their axial symmetry of geometry and loading condition. The region of filler was also meshed by 2D finite elements PLANE 183. Compressive action of the top steel plate was modelled by the prescribed maximum displacement applied on the surface of FE model at $y = 0$. Due to the symmetry of FE model, we assigned the displacements $U_y = 0$ at $x = 0$. The contact surfaces of the shells and bottom steel plate were meshed by contact elements CONTA 171 and TARGE 169, respectively. Figure 14 demonstrates the initial and deformed configurations of TTB filled with a

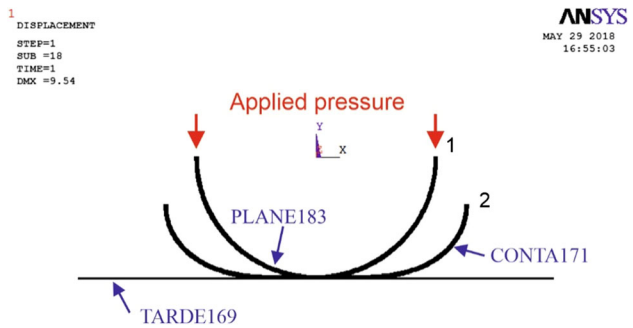

Figure 13 Initial **1** and deformed **2** configurations of hollow TTB.

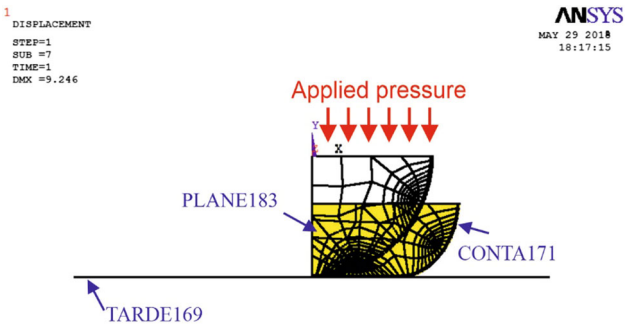

Figure 14 Initial (black) and deformed (yellow) configurations of TTB filled with a practically incompressible medium.

practically incompressible media at the maximum displacement of the top steel plate equalled to 8 mm.

The results of the simulation of compression behaviour of TTB shell filled with an incompressible medium are discussed below.

Empty and filled with the water TTB were tested in compression with a crosshead rate of 5 mm/min. Experimental and calculated force–displacement diagrams in compression are presented in Fig. 15.

It is seen that on the initial stage of loading, the strain depends only on the properties of the shell material and coincide for the filled and hollow systems and predicted by Reissner (1). Further, with increasing of load more than ca. 40–60 N, the strain depends much more on the filler and the calculated and experimental diagrams for the filled and hollow shells essentially differ. Good agreement of FEM calculation with experimental clearly validates the mechanical model for TTB system suggested.

Compression of a closed cylindrical shell-core system between two rigid plates

The second model shell was thin-walled Closed Cylindrical Shell (CCS), considered also in compression between two steel plates in the direction of shell diameter. CCS has the following geometrical dimensions R = 30 mm, h = 0.16 mm, h/R = 0.0053. Elastic properties of shell material were experimentally evaluated as $E = 3.90 \pm 0.24$ GPa, $\nu = 0.35$ in series of tensile tests of strip-shaped samples with sizes of 100 × 15 × 0.16 mm at crosshead displacement rate 10 mm/min. Hollow and filled with a practically incompressible medium (water) with elastic properties: E_f = 20.0 MPa, ν_f = 0.49967 CCS were tested and modelled.

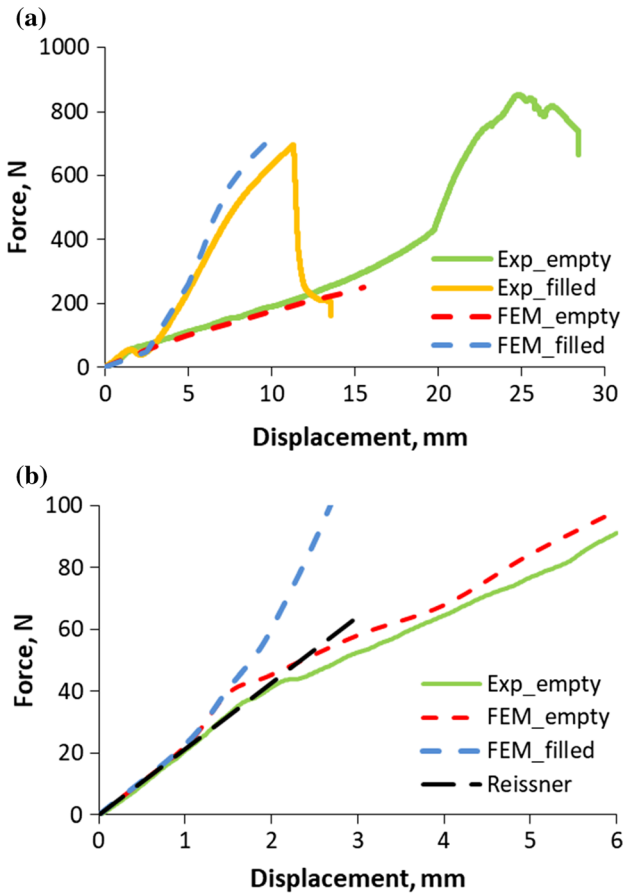

Figure 15 Force–displacement diagrams for the hollow and filled with the water model TTB system **a** and enlarged starting segment of the diagrams **b.** Experiment (solid lines, green for empty TTB and yellow for filled with water), FEM calculations (dashed lines, red for empty TTB and blue for filled with water), calculation by Reissner Eq. (1) (black dashed line).

Because we analyse a stress–strain state of the hollow CCS in the middle cylindrical part far from the ends neglecting the edge effects, the FEM model constructed for the hollow CCS was very similar to the FE model for hollow TTB (with the differences caused by the values of geometrical dimensions and elastic properties).

The results of FEM calculations for hollow CCS are also similar to those obtained for hollow TTB (see Fig. 13). However, due to the greater thinness of wall $h/R = 0.0053$, the hollow CCS had a larger deflection at the same maximum displacement 10 mm of the top steel plate.

FE modelling of CCS filled with a practically incompressible medium is the same as shown in Fig. 14. In this case, we also consider only a quarter of their cross sections owing to their axial symmetry of geometry and loading condition; other conditions are similar to TTB.

Compression tests of hollow and filled CCS were performed with a crosshead rate of 10 mm/min. Force–displacement diagrams in compression are given in Fig. 16. It is well seen that compression diagrams for hollow and filled CCS essentially differ. FEM calculations are in good agreement with the experimental results for both cases. Using Reissner Eq. (1) based on continuum elastic theory, it is possible to roughly evaluate the slope of the starting section for small strains that coincide for both kinds of the diagrams and is driven by the elasticity of the shell. Deformability of CCS for large strains mostly determines by volume changes of the shell and causes much stiffer behaviour of the shell filled with liquid than a hollow shell. CCS cross section in the unloaded state has a form of a circle that later under applied load is deformed to the form of the ellipse, i.e. volume of the CCS tends to reduce during compression experiment. These changes in volume are proportional to the change in the cross sectional area of the shell. It was assumed that the circumference of the shell is constant and deformation of cross section proceeds in a semiminor axis direction. Changes of the cross section area during deformation was calculated using the Ramanujan approximation [42] of the ellipse circumference (10)

$$l \approx \pi\left(3(a+b) - \sqrt{(3a+b)(a+3b)}\right) \tag{10}$$

where l is a circumference of an ellipse with semi-major axis a and semiminor axis b. The area of the cross section was calculated from (11):

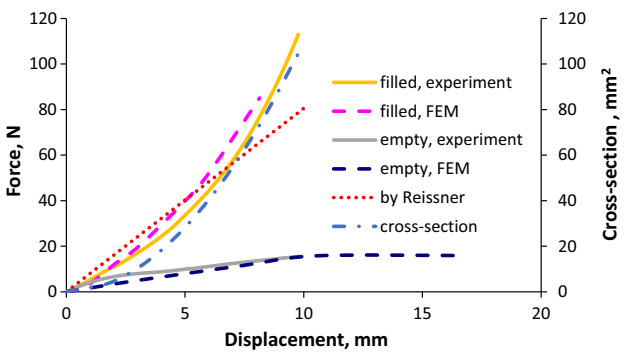

Figure 16 Force–displacement diagrams for the hollow and filled model CCS. Experimental results (solid lines) compared to FEM results (dashed lines). Analytical calculations by Reissner (1) (dotted line). Cross-sectional area changes in CCS calculated by Eq. (11) (dot-dash line).

$$S = \pi ab \tag{11}$$

where $a = \frac{3l-4\pi b+\sqrt{-20\pi^2 b^2+12\pi bl+3l^2}}{6\pi}$, with the further determination of the change in the cross-sectional area ds as shown in Fig. 16. Very good agreement between compression diagram force–displacement of filled shell and its volume decrease is clearly seen. This means that deformation behaviour of capsules filled with a liquid is driven mostly by volume changes of the capsule and compressibility of the filler neither the elastic properties of the shell material.

Analysing the diagrams in Figs. 15 and 16, the following remark has to be done. FE modelling and calculations of the filled TTB and CCS were carried out by using software ANSYS Mechanical 12.1 designed for structural analysis. We model water in TTB and CCS as a practically incompressible media with the elastic characteristics equalled to E_f = 20.0 MPa, ν_f = 0.49967. This rough but sufficient approximation allowed us to estimate the influence of "water-like" filler on deformation behaviour of the model shells considered and compare it with those of the hollow model shells.

Comparison of the force–displacement diagrams for hollow TTB and CCS with the diagrams for the filled model shells (see Figs. 15, 16) showed that a practically incompressible filler increases several times the applied force, which is required to realise the same deflection as in the case of hollow model shells. Comparison of the experimental and FEM calculated force–deflection diagrams testifies about well enough agreement for the hollow TTB and CCS, but a slightly worse for the filled ones. The latter circumstance was expected due to the approximation applied for modelling the water properties in the filled model shells. The numerical FEM results are agreed well enough with the results of tests carried out with model shells and the closed-form solution derived.

Thus, the proper FEM modelling can be used as an effective tool for solving the problems the thin-walled hollow and filled shells (microcapsules) accounting for their significant nonlinear deformation behaviour even though microcapsules shell material possess more brittle behaviour.

Compression of gelatine capsules

Oil-filled gelatine spherical capsules were one additional model system selected that allows us understanding the mechanical behaviour in compression of a shell filled with incompressible liquid. These capsules were prepared by thermal gelation method, adapted from [43], using D-glucose as a crosslinking agent, resulting in large and flexible spherical capsules, as desired. The size of the capsule was large enough to perform a mechanical test of the single capsule and also to cut the samples of shell material for individual tests. Compression tests were performed under the test speed of 2 mm/min. Capsules had a diameter of D = 9.7 ± 0.1 mm and wall thickness h = 0.45 mm. Samples of shell material for compression tests had a ring shape of approx. 5 mm height and were cut from a capsule sidewall. All tests were performed under laboratory conditions at T = 18 °C. Quasi-static diagrams of compression tests of shell samples are represented in Fig. 17 and elastic modulus of the material was evaluated as E = 4.6 ± 1.2 MPa.

The quasi-static diagrams of compression tests of oil-filled gelatine capsules and the calculated one by Reissner Eq. (1) are represented in Fig. 18. Once again, good agreement between compression diagram (force–displacement) of filled shell and continuum elastic theory calculation for starting segment of the diagrams when the elasticity of the shell material plays an essential role is clearly seen. Deformation behaviour of capsules filled with a liquid at larger strains is driven mostly by volume changes of the capsule and compressibility of the filler neither elastic properties of the shell material.

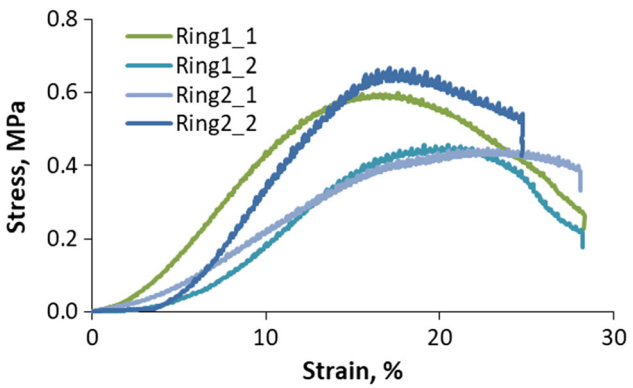

Figure 17 Quasi-static diagrams of four compression tests of gelatine capsule shell samples.

Conclusions

Mechanical behaviour of microcapsules for self-sensing polymer composites was characterised experimentally and modelled. SEM images and results of AFM testify that microcapsules of both types have a spherical form with average diameters of 7 and 2 μm and the wall thickness of 0.10 μm.

Stiffness and strength of single microcapsules were characterised experimentally by AFM and direct tests of macro samples of shell materials. Elastic modulus and compression strength of the shell material were evaluated from experiments and used for FE and analytical modelling. Comparison of results of micro- and macro-measurements indicate that the properties of the shell material strongly depend on manufacturing technology and storage conditions, and sometimes could be used only as estimations. Modelling of compression behaviour of microcapsules confirms that buckling of the spherical shell is a critical issue that defines mechanical limits of microcapsules applications. The difference of ca. 1% between the critical values calculated by FEM and closed-form solution proves the effectiveness of FEM application for describing the mechanical behaviour of the thin-walled hollow spherical shells under external pressure.

Three types of model shells were tested experimentally in compression and successfully modelled that allowed us to understand the mechanical behaviour of single microcapsules. Microcapsules should be considered as a complex structure whose mechanical behaviour should strongly depend on the properties of shell material and the liquid inside the capsule. The results obtained will be used for modelling of mechanical behaviour of smart polymer composites with embedded microcapsules applied for damage indication of materials.

Thus, the novelty of the research concerned with using the complex approach for analysis of physical and mechanical properties of microcapsules commercially produced by Papierfabric August Koehler. The approach includes experimental determination of the elastic and strength characteristics of microcapsules, their geometrical characterisation, and analytical and finite element modelling of nonlinear deformation behaviour of demonstration thin-walled shells. The verification of numerical results obtained with the FEM models developed and compression tests of the demonstration thin-walled shells is also the element of the paper novelty.

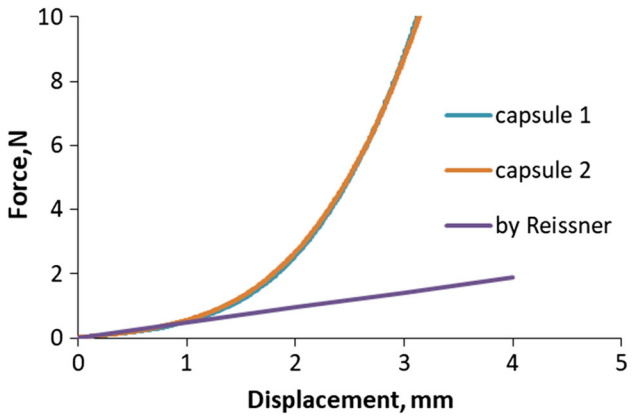

Figure 18 Quasi-static compression diagrams of gelatine capsules and calculation by Reissner Eq. (1).

Acknowledgements

This research is funded by the Latvian Council of Science, project DUROCAPS, Project No. lzp-2018/1–0084. This work has received funding from the European Union's Horizon 2020 research and innovation programme under the Marie Skłodowska-Curie grant agreements No 645662; was developed within the scope of the project CICECO-Aveiro Institute of Materials, UIDB/50011/2020 and UIDP/50011/2020, financed by national funds through the FCT/MEC and when appropriate co-financed by FEDER under the PT2020 Partnership Agreement.

Compliance with ethical standards

Conflict of Interest The authors declare that they have no conflict of interest.

References

[1] Bulderberga O, Aniskevich A, Vidinejevs S (2016) A glass–fiber-reinforced composite with a damage indication function. Mech Compos Mater 52(2):155–162

[2] Vavouliotis A, Paipetis A, Kostopoulos V (2011) On the fatigue life prediction of CFRP laminates using the electrical resistance change method. Compos Sci Technol 71:630–642

[3] Keulen C et al (2011) Embedded fiber optic sensors for monitoring processing, quality and structural health of resin transfer molded components. J Phys Conf Ser 305(1):012135

[4] Dragašius E et al (2015) The strength investigation of the composite material with implanted sensors. Mechanika 21(1):23–27

[5] Odom SA et al (2011) Visual Indication of Mechanical Damage Using Core-Shell Microcapsules. ACS Appl Mater Interfaces 12(3):4547–4551

[6] Keller MW, Sottos NR (2006) Mechanical properties of microcapsules used in a self-healing polymer. Exp Mech 46(6):725–733

[7] Sanada K, Itaya N, Shindo Y (2008) Self-healing of interfacial debonding in fiber-reinforced polymers and effect of microstructure on strength recovery. The Open Mech Eng J 2:97–103

[8] Wang Y, Pham DT, Ji C (2015) *Self-healing composites: A review*. Cogent. Engineering 2:1075686

[9] Ahmed A, Sanada K, Fanni M, El-Moneim AA (2018) A practical methodology for modeling and verification of self-healing microcapsules-based composites elasticity. Compos Struct. 184:1092–1098

[10] Gan SN, Shahabudin N (2019) Applications of microcapsules in self-healing polymeric materials. In Salaün F (ed) Microencapsulation—processes, technologies and industrial applications. IntechOpen

[11] Yuan L et al (2019) Preparation and characterization of microencapsulated ethylenediamine with epoxy resin for self-healing composites. Sci Rep 9(1):18834

[12] Xue C et al (2019) A review study on encapsulation-based self-healing for cementitious materials. Struct Concr 20(1):198–212

[13] Brown EN, White SR, Sottos NR (2004) Microcapsule induced toughening in a self-healing polymer composite. J Mater Sci 39(5):1703–1710. https://doi.org/10.1023/B:JMSC.0000016173.73733.dc

[14] Haghayegh M, Mirabedini SM, Yeganeh H (2016) Microcapsules containing multi-functional reactive isocyanate-terminated polyurethane prepolymer as a healing agent Part 1: synthesis and optimization of reaction conditions. J Mater Sci 51(6):3056–3068. https://doi.org/10.1007/s10853-015-9616-6

[15] He Z et al (2019) Self-healing isocyanate microcapsules for efficient restoration of fracture damage of polyurethane and epoxy resins. J Mater Sci 54(11):8262–8275. https://doi.org/10.1007/s10853-018-03236-3

[16] Vidinejevs S et al (2013) Development of a composite with an inherent function of visualization of a mechanical action. Mech Compos Mater 49(1):77–84

[17] Song Y-K et al (2015) A microcapsule-type fluorescent probe for the detection of microcracks in cementitious materials. Sens Actuators B Chem 222:1159–1165

[18] Li W et al (2016) Autonomous indication of mechanical damage in polymeric coatings. Adv Mater 28(11):2189–2194

[19] Bulderberga O, Aniskevich A (2017) Polymer composite material with inherent function of damage visual indication. In: Conference Paper, 21st International Conference on Composite Materials, ICCM 2017, Xi'an, China. August 2017, pp 20–25

[20] Geng J et al (2018) Damage-responsive microcapsules for amplified photoacoustic detection of microcracks in polymers. Chem Mater 30:2198–2002

[21] Zheng X et al (2020) Fabrication of self-reactive microcapsules as color visual sensing for damage reporting. J Mater Sci

[22] Zhang Q et al (2018) Review of recent achievements in self-healing conductive materials and their applications. J Mater Sci 53(1):27–46. https://doi.org/10.1007/s10853-017-1388-8

[23] Neubauer MP, Poehlmann M, Fery A (2014) Microcapsule mechanics: from stability to function. Adv Coll Interface Sci 207:65–70

[24] Fery A, Weinkamer R (2007) Mechanical properties of micro- and nanocapsules: single-capsule measurements. Polymer 48(25):7221–7235

[25] Bando K, Yamaguch Y (2017) Mechanical characterization of APA microcapsules by parallel-plate compression. J Membr Sep Technol 6:40–47

[26] Ghaemi A et al (2016) Mechanical behaviour of microcapsules and their rupture under compression. Chem Eng Sci 142:236–243

[27] Chen PW, Brignoli J, Studart AR (2014) Mechanics of thick-shell microcapsules made by microfluidics. Polymer 55:6837–6843

[28] Guadagno L et al (2016) Evaluation of the mechanical properties of microcapsule-based self-healing composites. Int J Aerosp Eng 2016:10

[29] Vinogradova OI, Lebedeva OV, Kim B-S (2006) Mechanical behavior and characterization of microcapsules. Annu Rev Mater Res 36(1):143–178

[30] Zhang GSZ (2001) Mechanical properties of melamine-formaldehyde microcapsules. J Microencapsul 18(5):593–602

[31] Sun G, Zhang Z (2002) Mechanical strength of microcapsules made of different wall materials. Int J Pharm 242(1):307–311

[32] Knoche S, Kierfeld J (2014) Osmotic buckling of spherical capsules. Soft Matter 10(41):8358–8369

[33] Diliunas S, Leisis V, Zeleniakiene D (2007) Investigation of stress homogenization near inner cavity in the polymer structure. Indian J Eng Mater Sci 14(6):408–413

[34] Zeleniakiene D et al (2018) Simulation of mechanical behaviour of polychloroprene/versatic acid vinyl ester/methyl methacrylate/2-ethylhexyl acrylate copolymer blend. Iran Polym J 27(2):97–103

[35] Liu KK, Williams DR, Briscoe BJ (1996) Compressive deformation of a single microcapsule. Phys Rev E 54(6):6673–6680

[36] ImageJ. Image processing and analysis in java (available - https://imagej.nih.gov/ij/index.html)

[37] Yuan L et al (2007) Synthesis and characterization of microencapsulated dicyclopentadiene with melamine–formaldehyde resins. Colloid Polym Sci 285(7):781–791

[38] Vol'mir AS (1967) Stability of deformed systems. Moscow: Nauka (In Russian)

[39] Vlasov VZ (1962) Selected works. General theory of shells. Moscow: Printing House of AN SSSR (In Russian), p 1

[40] Alfutov NA (2000) Stability of Elastic Systems. Springer, Berlin

[41] Zeleniakiene D et al. (2016) A numerical simulation of mechanical properties of smart polymer composite with microcapsules for damage sensing applications. In: ECCM17—17th European conference on composite materials. Munich, Germany

[42] Glaeser G, Stachel H, Odehnal B (2016) The universe of conics. From the ancient Greeks to 21st century developments. Springer, Berlin

[43] Hiwale P et al (2011) In Vitro release of lysozyme from gelatin microspheres: effect of cross-linking agents and thermoreversible gel as suspending medium. Biomacromol 12(9):3186–3193

Publisher's Note Springer Nature remains neutral with regard to jurisdictional claims in published maps and institutional affiliations.